Bone 127 (2019) 155–163

Contents lists available at ScienceDirect

Bone

journal homepage: www.elsevier.com/locate/bone

Full Length Article

Osteoblast-specific expression of *Panx3* is dispensable for postnatal bone remodeling

Timur A. Yorgan, Stephanie Peters, Michael Amling, Thorsten Schinke*

Department of Osteology and Biomechanics, University Medical Center Hamburg Eppendorf, Hamburg 20246, Germany

ARTICLE INFO

Keywords:
Osteoblast
Expression analysis
Panx3
Mouse model

ABSTRACT

Since cost-effective osteoanabolic treatment options remain to be established, it is relevant to identify specific molecules physiologically regulating osteoblast differentiation and/or activity that are principally accessible as drug targets. Specific or predominant gene expression in a given cell type often predicts a relevant function in the respective tissue. Thus, we aimed to identify genes encoding membrane-associated proteins with selective expression in differentiated osteoblasts. We therefore applied an unbiased approach, i.e. Affymetrix Gene Chip hybridization, to compare global gene expression in primary murine osteoblasts at two stages of differentiation. For the most strongly induced genes we analyzed their expression pattern in different tissues, which led us to identify known and unknown osteoblast differentiation markers with predominant expression in bone. One of these genes was *Panx3*, encoding a transmembrane hemichannel with ill-defined function in skeletal remodeling. To decipher the role of Panx3 in osteoblasts we first generated *Panx3-fl/fl* mice carrying a *Runx2-Cre* transgene. Using undecalcified histology followed by bone-specific histomorphometry we did not observe any significant difference between 24 weeks old Cre-negative and Cre-positive littermates. We additionally generated and analyzed mice with ubiquitous *Panx3* deletion, where a delay of endochondral ossification did not translate into a detectable skeletal phenotype after weaning, possibly explained by compensatory induction of *Panx1*. Of note, newborn *Panx3*-deficient mice displayed significantly reduced serum glucose levels, which was not the case in older animals. Our findings demonstrate that *Panx3* expression in osteoblasts is not required for postnatal bone remodeling, which essentially rules out its suitability as a target protein for osteoanabolic medication.

1. Introduction

The skeleton is a highly complex tissue being constantly remodeled, not only during development and growth, but also throughout adult life [1]. This physiologically relevant process, i.e. bone remodeling, is mediated by two antagonistically acting cell types, bone-forming osteoblasts and bone-resorbing osteoclasts [2,3]. A relative increase of bone resorption over bone formation is the cellular cause of osteoporosis, a detrimental disease defined by reduced bone mineral density and increased skeletal fracture risk [4]. At present, the vast majority of affected individuals are treated by anti-resorptive therapy, inhibiting either osteoclast differentiation (Denosumab) or function (bisphosphonates) [5]. In contrast, cost-effective osteoanabolic drugs, i.e. molecules stimulating bone formation, remain to be established, and the currently most widely available treatment by daily injection of a parathyroid hormone fragment (Teriparatide) is rarely applied due to restrictive guidelines and cost concerns [6,7]. Therefore, since osteoporosis is not only the most common bone remodeling disorder, but also one to the most prevalent diseases in the aged population, it is highly relevant to identify additional drug targets for osteoanabolic treatment.

The majority of known physiologically relevant molecules controlling bone remodeling were identified in the last two decades by molecular genetics [8]. For instance, the combined analysis of patients with rare inherited skeletal disorders and the respective mouse deficiency models have led to the discovery of the pro-osteoclastogenic cytokine Rankl and its decoy receptor Opg, two key molecules controlling bone resorption [9]. Likewise, similar methodology enabled the identification of the putative Wnt co-receptor Lrp5 and its osteocyte-derived antagonist Sclerostin as major regulators of osteoblast activity [10]. These latter findings have also paved the way to establish a novel osteoanabolic treatment option for osteoporosis, i.e. monoclonal antibodies neutralizing the function of Sclerostin [11]. Importantly however, as long as this type of treatment is not available in clinical practice, there is an urgent need to identify additional molecules as putative drug targets for osteoanabolic medication.

Our experimental strategy was to utilize an unbiased approach to

* Corresponding author.
E-mail address: schinke@uke.de (T. Schinke).

https://doi.org/10.1016/j.bone.2019.06.008
Received 26 March 2019; Received in revised form 7 June 2019; Accepted 12 June 2019
Available online 14 June 2019

screen for genes with predominant expression in differentiated osteoblasts, whose function in bone remodeling could then be assessed by generating respective mouse deficiency models. Here we particularly focused on genes encoding membrane-associated proteins, since these should be best accessible for pharmacologic treatment. This approach led to the identification of the *Panx3* gene, whose osteoblast-specific expression pattern was confirmed by qRT-PCR. Since *Panx3*-deficient mice have been reported to display disturbed endochondral ossification at an early postnatal stage, we generated mice with specific *Panx3* inactivation in osteoblasts (*Panx3*$^{fl/fl;Runx2\text{-}Cre}$). Using undecalcified histology and bone-specific histomorphometry, however, we failed to detect relevant differences towards *Panx3*$^{fl/fl}$ littermate controls. We also did not observe a skeletal phenotype in 4 and 24 weeks old *Panx3*-deficient mice, albeit these displayed delayed ossification at birth. Taken together, our data demonstrate that Panx3, despite being predominantly expressed in differentiated osteoblasts, is dispensable for postnatal bone remodeling.

2. Materials and methods

2.1. Primary osteoblasts

Primary murine osteoblasts were isolated by sequential collagenase digestion from the calvariae of 5 days old mice as described [12]. After removal of the co-purified macrophage-like cells by CD11b-immunoaffinity [13,14] cells were plated and cultured in α-MEM until they reached 80% confluency (day 0). We then added ascorbic acid (50 μg/ml) and β-glycerophosphate (10 mM) to the cultures to induce osteogenic differentiation. RNA was isolated at various stages of differentiation and subjected to Affymetrix Gene Chip hybrization (day 5 and day 12) or qRT-PCR expression analysis (day 0, 4, 7, 10, 15, 20 or 25 of differentiation).

2.2. Expression analysis

RNA from murine tissues (from 10 weeks old C57Bl/6 mice) or cultured osteoblasts was isolated using the RNeasyMini kit (Qiagen, Germany). DNase digestion was performed according to manufacturer's instructions. Concentration and quality of RNA were measured using a NanoDrop ND-1000 system (NanoDrop Technology, USA). For genome-wide expression analysis, 5 μg of RNA were used for first strand cDNA synthesis. Synthesis of biotinylated cRNA was carried out using the IVT Labeling Kit (Affymetrix). For Gene Chip hybridization, the fragmented cRNA was incubated in hybridization solution at 45 °C for 16 h, before the Gene Chips (Affymetrix MG 430 2.0) were washed using the Affymetrix Fluidics Station 450. The raw data sets were deposited in GEO under accession code GSE71565 [15]. For RT-PCR expression analysis 500 ng of RNA was reversed transcribed using Verso cDNA Kit (Thermo Fisher Scientific Inc., USA) according to manufacturer's instructions. Gene-specific primers (Table S1) were used to amplify cDNA fragments of specific genes. For quantitative PCR analysis predesigned TaqMan assays (Applied Biosystems) and Taqman gene expression mastermix (Applied Biosystems) were used for *Panx1*, *Panx2*, *Panx3*,*Gja1*,*Gja3*, *Gja4*, *Gja5*, *Gjc1*, *Bglap*, *Slc2a1*, *Ibsp*, *Col1a1*, *Sost*, *Calcr*, *Tnfsf11* or *Acp5*. *Gapdh* expression was used as an internal control. Relative quantification was performed according to the $\Delta\Delta C_T$ method, and results were expressed in linear form using the formula $2^{-\Delta\Delta CT}$ for. Alternatively, quantification relative to *Gapdh* was applied for individual samples. The applicable method is stated in the figure legends.

2.3. Mouse models

Panx3$^{fl/fl}$ (Panx3$^{tm1a(KOMP)Wtsi}$) mice were obtained from the Mouse Biology Program (MBP), University of California, Davis, USA. Their genotyping was performed using primers 5′-GAG ATG GCG CAA CGC AAT TAA TG-3′ and 5′-GGA GGT GGA TTC TAT GCT CAC ACC C-3′ detecting a 343 bp *Panx3*^{fl} allele. *Runx2-Cre* transgenic mice and their genotyping have been described previously [16]. They carry an integrated bacterial artificial chromosome covering the *Runx2* locus with inserted Cre-coding sequence, which does not interfere with endogenous *Runx2* expression. Despite Runx2 activity in growth plate chondrocytes, our previous analyses have confirmed the efficacy of the *Runx2-Cre* transgene for gene inactivation in the osteoblast lineage [16–21]. To rule out any influence of genetic background we only analyzed Cre-positive and Cre-negative *Panx3*$^{fl/fl}$ littermates in the present study. *CMV-Cre* transgenic mice (B6·C-Tg(CMV-cre)1Cgn/J) were obtained from the live repository of the University Medical Center Hamburg-Eppendorf research animal facility. To allow ubiquitous deletion of *Panx3* these mice were mated with *Panx3*$^{fl/fl}$ mice. Genotyping for the recombined Panx3 allele was performed using primers 5′- AAG CCT GTA ACC TCT ATG GCA GTC C-3′ and 5′- GGA GGT GGA TTC TAT GCT CAC ACC C-3′ detecting a 866 bp *Panx3*-KO allele. As a loading control an unrelated genomic region was amplified using the primers 5′-AGA TCT CAG GCC CAT GGA GCA G-3′ and 5′-ATG GCT AAG GAG TCC TGA AC-3′. All mice were kept in a specific pathogen-free environment with a 12-hour light/dark cycle, 45–65% relative humidity and 20–24 °C ambient temperature in open or individually ventilated cages with wood shavings bedding and nesting material in groups not surpassing 6 animals. The mice had access to tap water and standard rodent chow (1328P, Altromin Spezialfutter GmbH & Co. KG, Germany) ad libitum. All animal experiments were approved by the animal facility of the University Medical Center Hamburg-Eppendorf and by the "Amt für Gesundheit und Verbraucherschutz" (Org529).

2.4. Skeletal analysis

After sacrifice the dissected skeletons were fixed in 3.7% PBS-buffered formaldehyde for 18 h at 4 °C, before they were stored in 80% ethanol. For μCT analysis, one femur of each mouse was extracted and excess soft tissue removed. μCT scanning and evaluation was performed with a voxel resolution of 10 μm as previously described using a μCT 40 desktop cone-beam microCT (Scanco Medical, Switzerland) [22] according to standard guidelines [23]. Trabecular bone was analyzed in the distal metaphysis in a volume situated 2500 μm to 500 μm proximal of the distal growth plate. Cortical bone was analyzed in a 1000 μm long volume situated in the middle of the diaphysis. The implemented thresholds were 300 and 250 for trabecular and cortical bone respectively. For bone histology, the lumbar vertebral bodies L3 to L6 and one tibia of each mouse were dehydrated in ascending alcohol concentrations and then embedded in methylmetacrylate as described previously [21]. Sections of 5 μm thickness were cut in the sagittal plane on a Microtec rotation microtome (Techno-Med GmbH, Germany) and stained by toluidine blue and vonKossa/van Gieson staining procedures as described [24]. Histomorphometry was performed according to the ASBMR guidelines [25] using the OsteoMeasure histomorphometry system (Osteometrics Inc., USA). For whole skeleton staining, newborn mice were sacrificed and the soft tissues were mechanically removed as far as possible. After fixation in 95% ethanol over night the skeletons were stained for 48 h in 0.015% alcian blue solution containing 20% acetic acid and 75% ethanol. Subsequently, the skeletons were washed for 3 h in 95% ethanol before residual soft tissue was removed by incubating them for 48 h in 2% KOH solution, before staining them over night with 0.005% alizarin red in an aqueous 1% KOH solution. Tissue transparency was achieved by incubation for at least 24 h in 20% glycerol, 1% KOH. Finally, the skeletons were stored in 50% glycerol, 47.5% ethanol.

2.5. Serum analysis

Glucose levels were determined at sacrifice using the Accu-Chek system (Roche Diabetes Care Deutschland GmbH, Germany).

2.6. Statistical analysis

All data presented in the manuscript were obtained from the analysis of littermates and are presented as means ± standard deviations. Group sizes are indicated in the figure legends. Statistical analysis was performed using unpaired, two-tailed Student's *t*-test with Bonferroni correction for multiple testing. Allele frequencies were tested against the expected distribution via Chi^2-test and survival curves were compared via a log-rank (Mantel-Cox) test utilizing Prism software (GraphPad Software Inc., USA). p-Values below 0.05 were considered statistically significant.

3. Results

To identify genes with differential expression during primary osteoblast differentiation we isolated macrophage-depleted primary calvarial osteoblast cultures [13,14] and differentiated them in the presence of ascorbic acid and ß-glycerophosphate for 5 and 12 days, respectively. RNA was subjected to Affymetrix Gene Chip hybridization, and genes were sorted according to their signal log ratio (SLR) between day 5 and day 12 of differentiation. Among the 100 genes with the highest level of induction we found several known markers of osteoblastogenesis and/or genes with relevance in bone biology (Table S2). As the main intention of our study was to identify additional regulators of bone remodeling, we next determined the tissue expression pattern of the 100 genes with the highest SLR by RT-PCR. Here we focused on nine different tissues, including femur and calvaria (Fig. 1). We observed predominant bone expression of several genes with previously reported bone-specific expression, such as *Phex*, *Ifitm5*, *Bglap*, and others [26–28], in addition to several genes whose function in osteoblasts was not fully defined at the time of our analysis. Taking into consideration the suitability as a potential drug target, we focused our next screening step on genes encoding membrane-associated proteins.

Here we applied qRT-PCR on sixteen different tissues, including spine, femur and calvaria. Whereas *Slc16a3*, *Sgms2*, *Slc13a1*, *Hhip*, *Fat3* and *Gpr133* were not exclusively expressed in skeletal tissues (Fig. S1), we observed predominant bone expression for the *Panx3* gene. In fact, similar to *Bglap*, encoding the well-established osteoblast marker Osteocalcin, robust *Panx3* expression was only detected in spine, femur and calvaria (Fig. 2A). In contrast, we found that *Panx1* was expressed in various tissues, whereas *Panx2* expression was most pronounced in the hypothalamus. We additionally monitored the expression of *Bglap* and *Panx* genes during the course of primary osteoblast differentiation (Fig. 2B). Here we observed the highest expression levels (when normalized to *Gapdh*) for *Panx3*, which was the only *Panx* gene displaying differential expression during the course of osteoblastogenesis. Taken together, these findings demonstrated that *Panx3* is an osteoblast differentiation marker with predominant expression in bone, thereby raising the hypothesis that its physiological function is related to bone remodeling.

To analyze this function we took advantage of commercially available ES cell clones that were utilized to generate mice with a floxed *Panx3* allele. Since it was reported, at the time of our analyses, that *Panx3*-deficient mice display skeletal abnormalities at birth [29,30], we decided to cross the *Panx3*$^{fl/fl}$ mice with *Runx2-Cre* mice in order to obtain specific deletion in osteoblasts [16]. We observed that *Panx3*$^{fl/fl;Runx2\text{-}Cre}$ mice were born at the expected Mendelian ratio and that they did not display gross abnormalities. To assess the Cre-mediated recombination specificity in *Panx3*$^{fl/fl;Runx2\text{-}Cre}$ mice we applied genomic PCR on DNA from different tissues using primers amplifying the recombined *Panx3* fragment. Here we observed the strongest signals on skeletal tissues as well as in cultured primary osteoblasts at day 15 of differentiation (Fig. 3A). We next analyzed the *Panx3*$^{fl/fl;Runx2\text{-}Cre}$ mice for potential bone remodeling abnormalities at 24 weeks of age, compared to *Panx3*$^{fl/fl}$ littermates. Using µCT imaging of the femoral bones we observed that parameters of trabecular bone mass were not significantly different between *Panx3*$^{fl/fl;Runx2\text{-}Cre}$ mice and *Panx3*$^{fl/fl}$ littermate controls, whereas cortical thickness was slightly reduced in the *Panx3*$^{fl/fl;Runx2\text{-}Cre}$ mice (Fig. 3B,C). Similarly, there was no detectable trabecular bone abnormality observed in *Panx3*$^{fl/fl;Runx2\text{-}Cre}$ mice as assessed by static histomorphometry on undecalcified spine sections (Figs. 3D,E; S2). Cellular and dynamic histomorphometry performed on the same sections demonstrated that *Panx3*$^{fl/fl;Runx2\text{-}Cre}$ mice display normal numbers of osteoclasts, osteocytes and osteoblasts, as well as a normal bone formation rate compared to *Panx3*$^{fl/fl}$ littermate controls (Fig. 3F).

To circumvent the potential problem of residual Panx3 activity in *Panx3*$^{fl/fl;Runx2\text{-}Cre}$ mice we also generated *Panx3*$^{+/-}$ mice after ubiquitously deleting one allele by crossing the *Panx3*$^{fl/fl}$ mice with *CMV-Cre* mice. We then mated *CMV-Cre*-negative *Panx3*$^{+/-}$ mice and analyzed the offspring for the presence of *Panx3*-deficient animals (Fig. 4A). We hereby observed that 30% of the *Panx3*$^{-/-}$ mice died shortly after birth, whereas all surviving animals reached the age of 24 weeks without displaying gross abnormalities (Fig. 4B). Moreover, similar to *Panx3*$^{fl/fl;Runx2\text{-}Cre}$ mice, there was no change in trabecular bone mass, quantified in vertebral body sections at the age of 4 weeks, in *Panx3*$^{-/-}$ mice compared to wildtype littermate controls (Figs. 4C,D, S3A). Likewise, at the age of 24 weeks the *Panx3*$^{-/-}$ mice showed no structural skeletal abnormalities as determined by µCT analysis of the femur, yet there was a moderate reduction in femur length (Fig. 4E,F). Most importantly however, undecalcified histology of spine sections (Figs. 4G, S3B) followed by quantitative histomorphometry (Figs. 4H, S4) clearly demonstrated the absence of a bone remodeling phenotype in 24 weeks the *Panx3*$^{-/-}$ mice.

We next analyzed the newborn mice for disturbances of skeletal development or potential causes of postnatal lethality. In fact, while the number of *Panx3*$^{-/-}$ embryos did not significantly deviate from the expected Mendelian ratio at E19.5, the number of *Panx3*$^{-/-}$ mice was remarkably decreased three days after birth (Fig. 5A). Consistent with previous reports we also observed decreased length and severe morphological deformities of the long bones of one-day old *Panx3*$^{-/-}$ mice (Fig. 5B), indicating a defect of endochondral ossification, which was confirmed in undecalcified spine sections (Fig. 5C). On the other hand, the observed abnormalities were not apparently lethal, thereby raising the question, if they explain the high mortality rate of newborn *Panx3*$^{-/-}$ mice. Of note, early perinatal lethality, due to hypoglycemia, without major defects on the skeleton has previously been reported for a mouse model with an osteoblast-specific deletion of *Ptprv*, encoding a protein tyrosine phosphatase regulating osteoblast-controlled glucose homeostasis [31]. This led us to determine random fed serum glucose concentrations in 1 day and 4 weeks old animals. We thereby observed a significant decrease in newborn *Panx3*$^{-/-}$ mice, yet serum glucose levels were not different between wildtype, *Panx3*$^{+/-}$ and *Panx3*$^{-/-}$ mice at 4 weeks of age (Fig. 5D).

We finally applied qRT-PCR to monitor gene expression in calvarial bone from *Panx3*$^{-/-}$ embryos at 19.5 dpc. Compared to wildtype controls, there was an increased expression of *Panx1* in *Panx3*-deficient embryos, suggesting that the loss of Panx3 can be compensated by induction of *Panx1* (Fig. 5E). We also analyzed for a compensatory induction of connexin-encoding genes with putative impact on the skeleton [32]. Here we did not observe an induction of gene expression in *Panx3*-deficient embryos, yet *Gja3* was expressed at significantly lower levels. Importantly, the strongest induction of gene expression in *Panx3*$^{-/-}$ embryos was observed for *Slc2a1* (Fig. 5F), encoding the glucose transporter Glut1, whose critical function in osteoblasts was previously demonstrated [33]. In contrast, markers of osteoblast (*Bglap*, *Ibsp*, *Col1a1*, *Sost*, *Tnfsf11*) or osteoclast lineage cells (*Calcr*, *Acp5*) were not differentially expressed. Taken together, our findings demonstrate that Panx3 expression in osteoblasts is dispensable for bone remodeling regulation, yet it might be relevant in the context of the endocrine functions mediated by skeletal remodeling cell types [34].

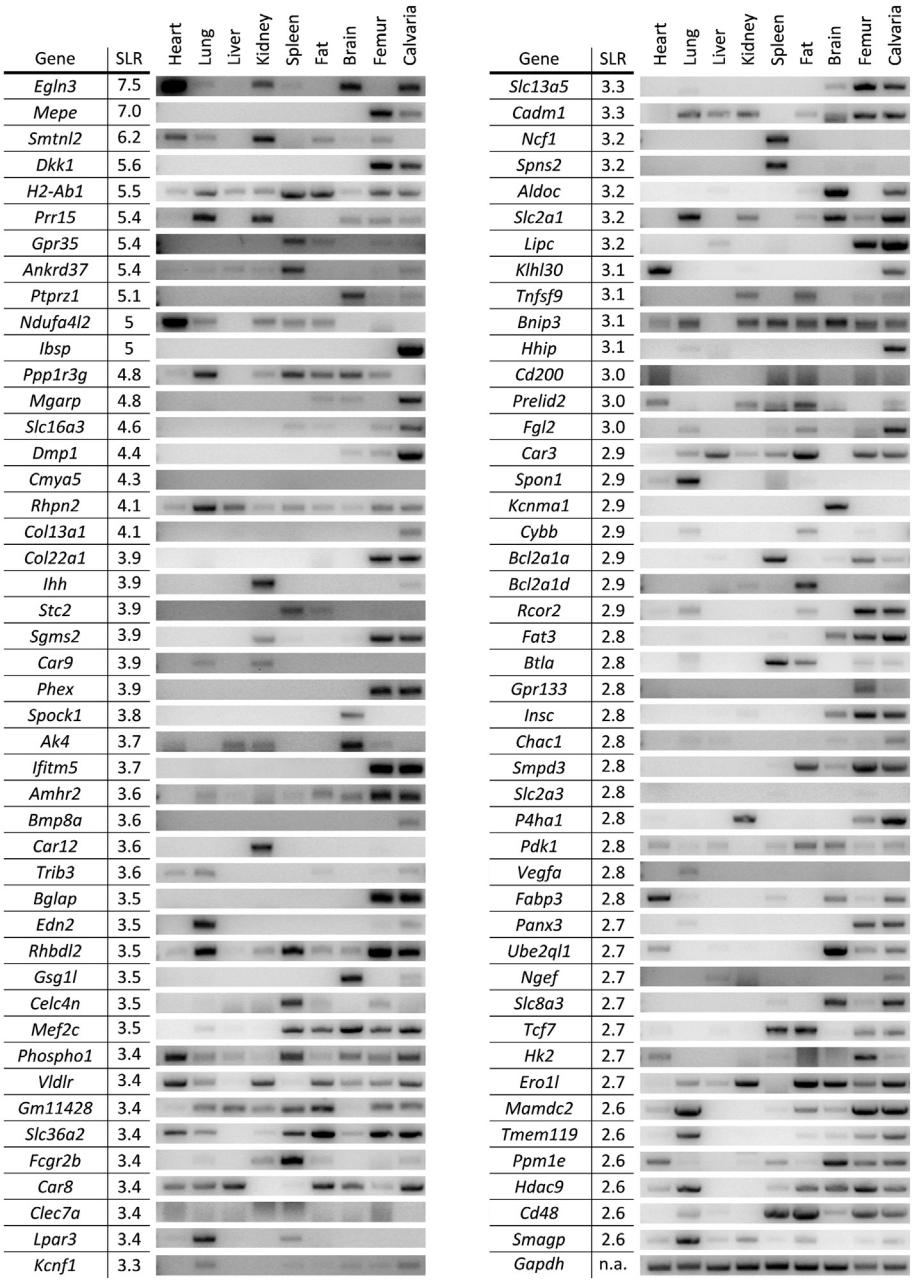

Fig. 1. Tissue expression pattern of genes induced during osteoblast differentiation. The expression pattern of the 100 most strongly induced genes, as determined by Gene Chip hybridization comparing primary calvarial osteoblasts at day 5 and day 12 of differentiation, were analyzed for their expression in the indicated tissues. *Gapdh* expression was monitored as positive loading control.

4. Discussion

Specific or predominant gene expression in a given cell type often predicts a relevant function in the respective tissue. In the case of the osteoblast lineage, there are several examples for genes with restricted expression pattern, whose inactivation causes a skeletal disorder. These include, among others, the osteoblast-specific transcription factor Sp7, the transmembrane protein Ifitm5, the endopeptidase Phex, or the osteocyte-derived Wnt signaling antagonist Sclerostin [26,27,35,36]. From a pharmacological perspective it is indeed relevant that Sclerostin is not ubiquitously expressed, since potential side effects of antibody-mediated Sclerostin neutralization should be limited. Although this notion was principally supported in ongoing clinical trials [11,37,38], there is increasing evidence not only for additional *Sost* expression sites, but also for other roles of Sclerostin beyond inhibition of bone formation [39,40]. Based on these arguments the aim of our study was to utilize an unbiased approach to screen for additional genes with predominant expression in differentiated osteoblasts, whose function in bone remodeling could then be assessed by generating respective mouse deficiency models.

Using a fully unbiased approach, i.e. genome-wide expression analysis followed by expression analysis in different tissues, we identified *Panx3* as a gene encoding a transmembrane protein with predominant expression in osteoblasts, whose function in bone remodeling was ill-defined. In our opinion it is important to state that the chosen strategy also picked up several genes with known key functions of osteoblasts of mice and humans, such as *Bglap*, *Phex* or *Ifitm5*, thereby underscoring the principal value of our approach. Panx3 is known to form hemichannels facilitating the passage of Ca^{2+} or ATP [41,42]. Its function in osteoblasts was not defined at the beginning of our functional studies,

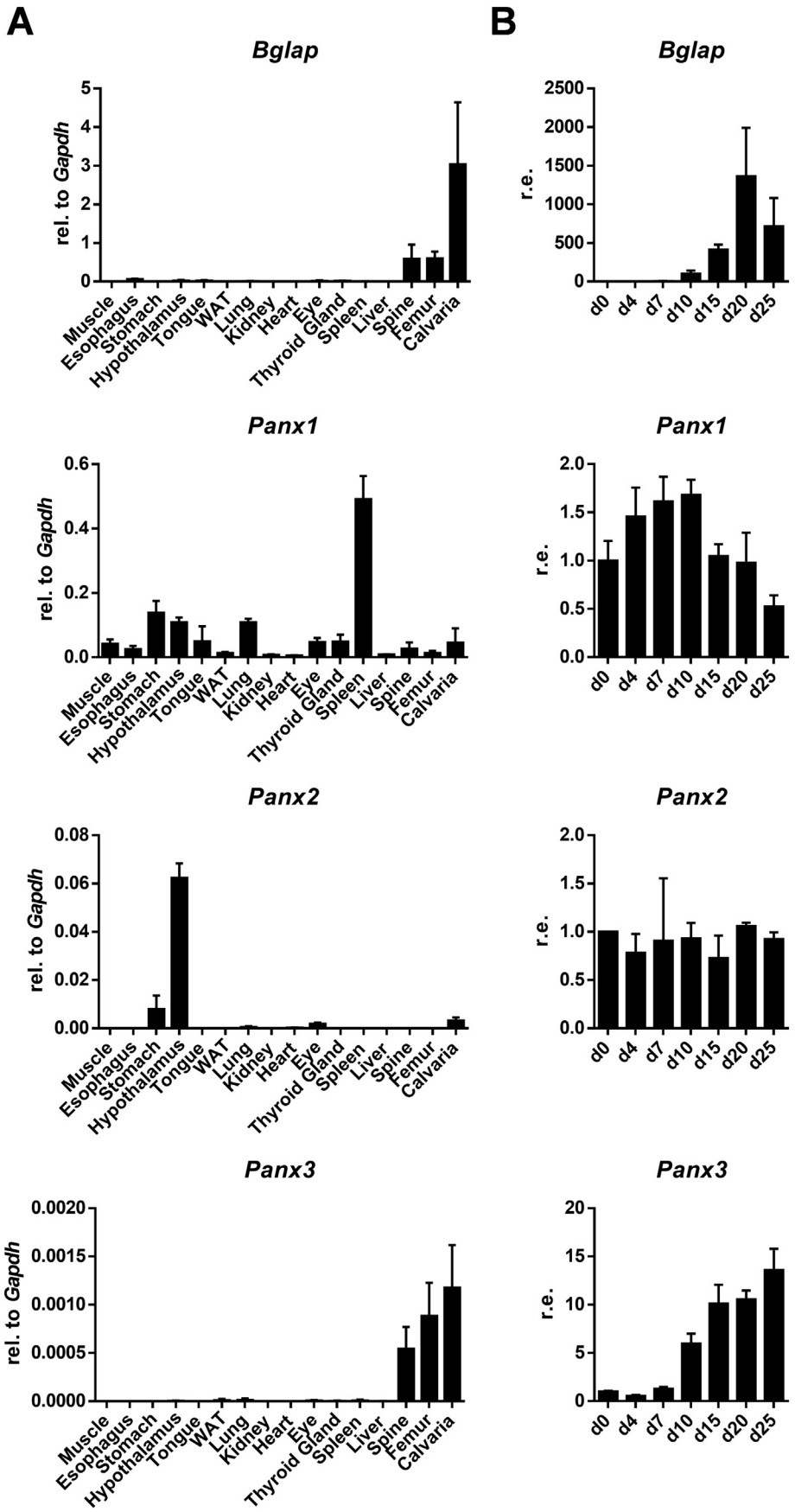

Fig. 2. Extended expression pattern for *Panx* genes. (A) qRT-PCR expression analysis for *Bglap*, *Panx1*, *Panx2* and *Panx3* in the indicated tissues. Shown is the expression relative to the respective *Gapdh* expression. n = 3 samples per tissue. (B) qRT-PCR expression analysis for the same genes in primary calvarial osteoblasts at the indicated days of differentiation. Shown is the expression relative to day 0 of differentiation. n = 3 samples per timepoint.

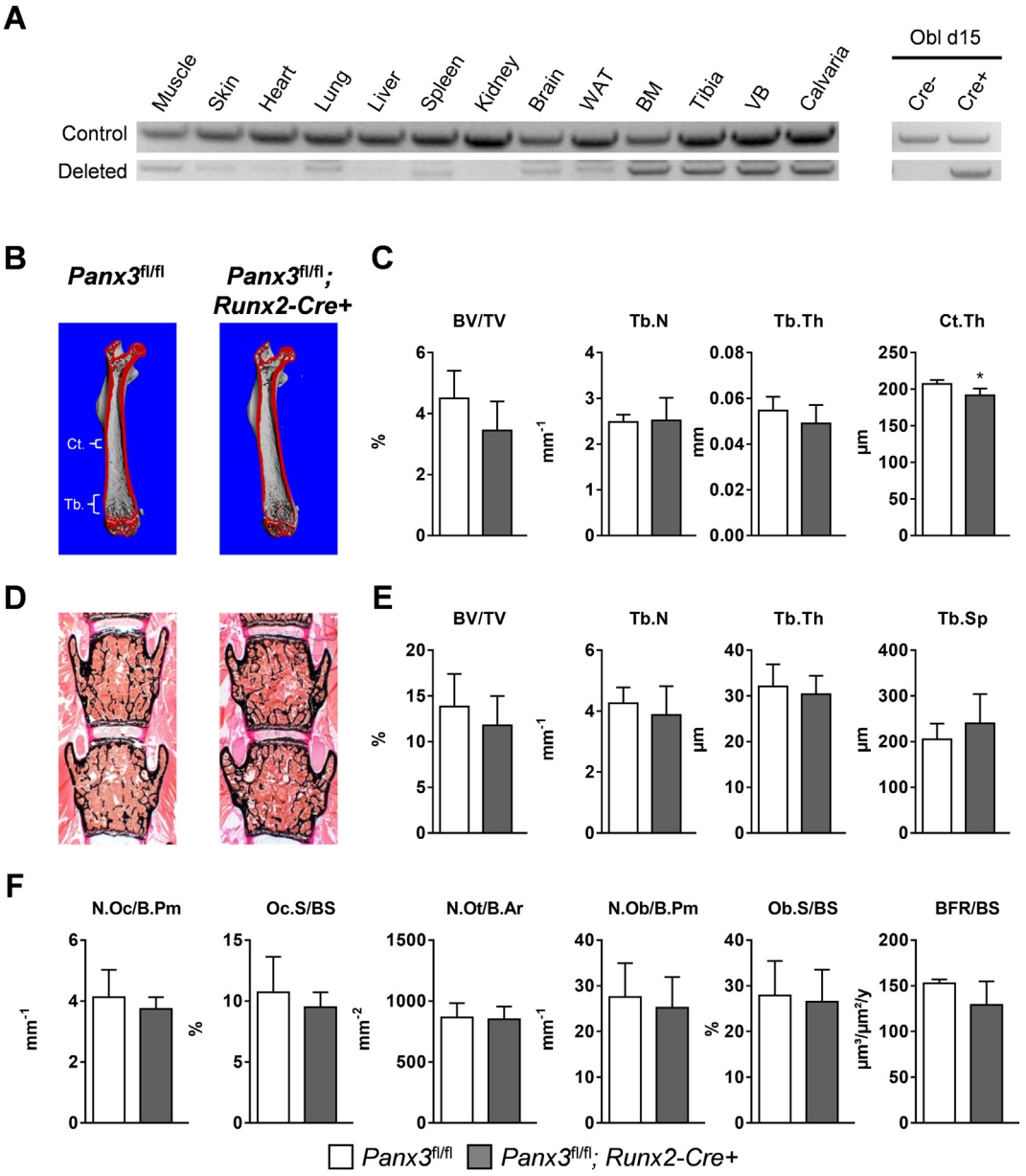

Fig. 3. Skeletal phenotype of *Panx3*$^{fl/fl;Runx2\text{-}Cre}$ mice. (A) Analysis of the recombination specificity by genomic PCR amplifying either an unrelated genomic region (control) or the recombined *Panx3* gene (deleted). Genomic DNA was extracted from the indicated organs or differentiated calvarial osteoblasts from *Panx3*$^{fl/fl;Runx2\text{-}Cre}$ mice. (B) Representative μCT images of the femora from 24 weeks old female *Panx3*$^{fl/fl}$ and *Panx3*$^{fl/fl;Runx2\text{-}Cre}$ mice. The virtual cutplane appears red. Regions evaluated for trabecular (Tb.) and cortical (Ct.) parameters are indicated by the white markings. (C) Structural parameters of skeletal microarchitecture from the same femora as determined by μCT evaluation. (D) Representative undecalcified histological sections of vertebral bodies from 24 weeks old, female *Panx3*$^{fl/fl}$ and *Panx3*$^{fl/fl;Runx2\text{-}Cre}$ mice. Von Kossa/van Gieson stain. (E) Histomorphometric evaluation of trabecular bone parameters in the same sections. (F) Histomorphometric evaluation of cellular and dynamic bone remodeling parameters in the same sections. Data were analyzed by Student's *t*-test. n = 5 mice per group. *p < 0.05 vs. *Panx3*$^{fl/fl}$. (For interpretation of the references to colour in this figure legend, the reader is referred to the web version of this article.)

yet even after the description of a skeletal phenotype in newborn *Panx3*-deficient mice, its role in postnatal bone remodeling remained to be elucidated. More specifically, *Panx3*-deficient mice have been shown to display impaired endochondral ossification at the newborn stage, which was attributed to increased proliferation of osteoprogenitors and chondrocytes of the growth plate [29,30]. Within this latter region it was also found that terminal differentiation into hyperthrophic chondrocytes was impaired in the absence of Panx3 [30]. Overall, these alterations of chondrocyte proliferation and differentiation have been reported to result in a reduction of bone length that we were able to confirm in the present manuscript. Furthermore, Panx3 deficiency has been reported to exert a protective effect in a surgically induced mouse model of osteoarthritis, suggesting a function of Panx3 in articular cartilage in addition to the growth plate [43]. Finally, the loss of the Panx3 gene has been found to result in subtle but significant changes in the overall morphology of femora and humeri from mature mice [44].

In this context it is also relevant to state that *Panx3* transcription was found to be promoted by the transcription factor Runx2, whose endogenous expression is however not affected in the *Runx2-Cre* transgenic mice [16,45]. The transcriptional regulation by Runx2 also explains the induction of *Panx3* expression during osteoblastogenesis, yet there is an apparent inconsistency in the precise timing between our study and previously published data. In fact, while others have reported that *Panx3* expression is only transiently increased in the course of primary calvarial osteoblast differentiation [30], we did not observe a decline of *Panx3* expression at later stages. Since it is generally difficult

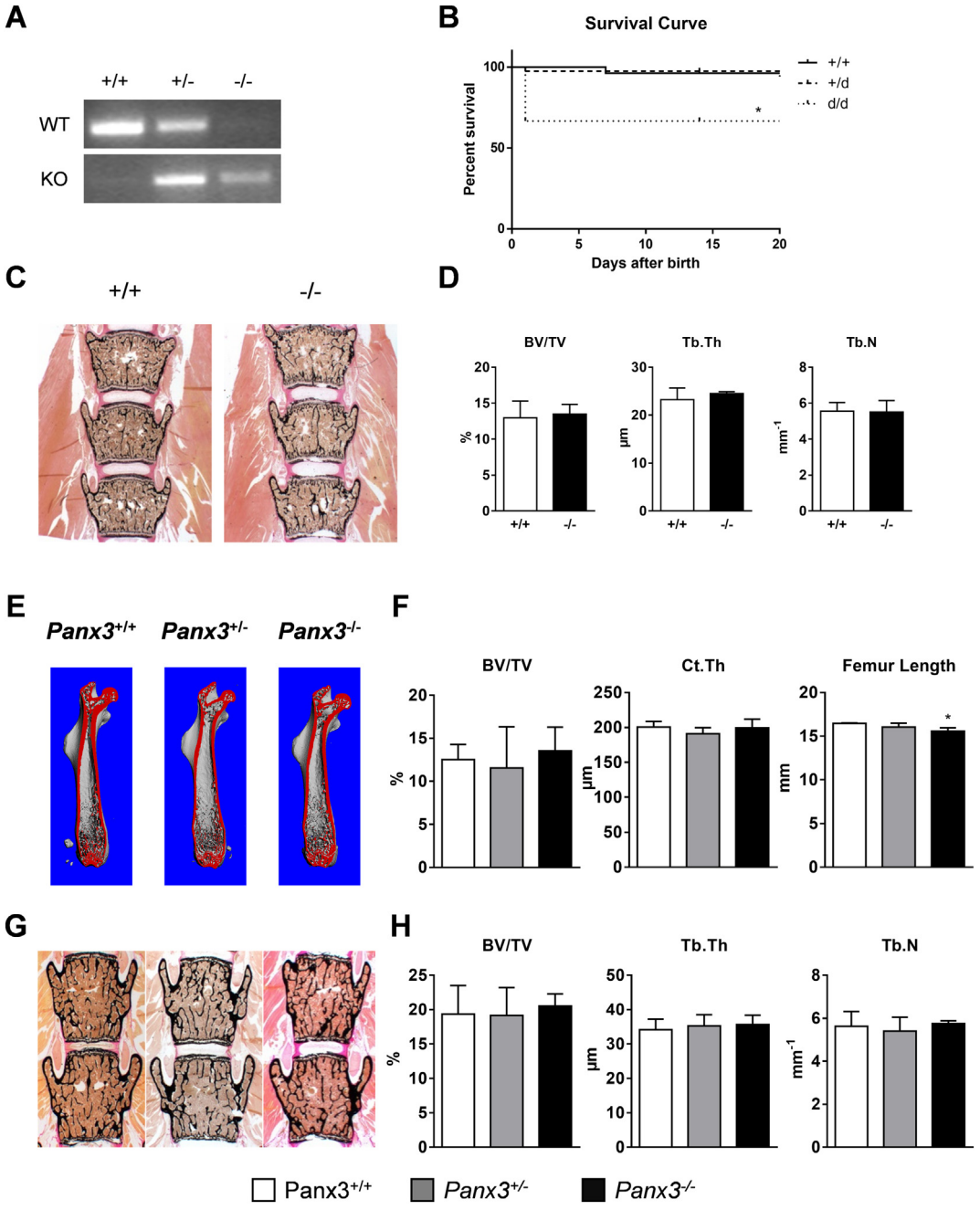

Fig. 4. Skeletal phenotype of *Panx3*-deficient mice. (A) Representative gel images of a genotyping PCR identifying wildtype, $Panx3^{+/-}$ and $Panx3^{-/-}$ mice. (B) Survival curve of mice grouped by *Panx3* genotype. Data were analyzed by log-rank (Mantel-Cox) test. n = 26 ($Panx3^{+/+}$), 39 ($Panx3^{+/-}$), 9 ($Panx3^{-/-}$).*p < 0.05 vs. $Panx3^{+/+}$. (C) Representative undecalcified histological sections of vertebral bodies from 4 weeks old, female $Panx3^{+/+}$ and $Panx3^{-/-}$ mice. Von Kossa/van Gieson stain. (D) Histomorphometric evaluation of trabecular parameters in the same sections. Data were analyzed by Student's *t*-test. n = 7 ($Panx3^{+/+}$), 4 ($Panx3^{-/-}$).*p < 0.05 vs. $Panx3^{+/+}$ (E) Representative µCT images of the femora from 24 weeks old, male $Panx3^{+/+}$, $Panx3^{+/-}$ and $Panx3^{-/-}$ mice. The virtual cutplane appears red. (F) Structural parameters of skeletal microarchitecture of femora from the same mice determined by µCT evaluation. Data were analyzed by Student's *t*-test with Bonferroni correction for multiple testing. n = 3 ($Panx3^{+/+}$), 3 ($Panx3^{+/-}$), 5 ($Panx3^{-/-}$).*p < 0.05 vs. $Panx3^{+/+}$ (G) Representative undecalcified histological sections of vertebral bodies from 24 weeks old, male $Panx3^{+/+}$, $Panx3^{+/-}$ and $Panx3^{-/-}$ mice. Von Kossa/van Gieson stain. (H) Histomorphometric evaluation of trabecular parameters in the same sections. Statistical analysis and sample size was the same as in subpanel F. (For interpretation of the references to colour in this figure legend, the reader is referred to the web version of this article.)

to provide a full explanation for specific differences between own and published data we can only speculate that lower concentrations of ß-glycerophosphate and/or removal of macrophages, both applying for the present study, may be relevant in this context. In any case, although there was strong evidence for a critical function of Panx3 in osteoblast lineage cells, a histomorphometric analysis of bone remodeling has not yet been reported for adult *Panx3*-deficient mice.

By generating mice lacking Panx3 either in the osteoblast lineage or ubiquitously we could clearly demonstrate that *Panx3* expression in osteoblasts is dispensable for postnatal bone remodeling. One possible explanation for the lack of a significant difference between $Panx3^{fl/fl;Runx2\text{-}Cre}$ and $Panx3^{-/-}$ mice towards the respective littermate controls is that Panx1 could compensate for the loss of Panx3 activity. Of note, the opposite has previously been suggested by the analysis of

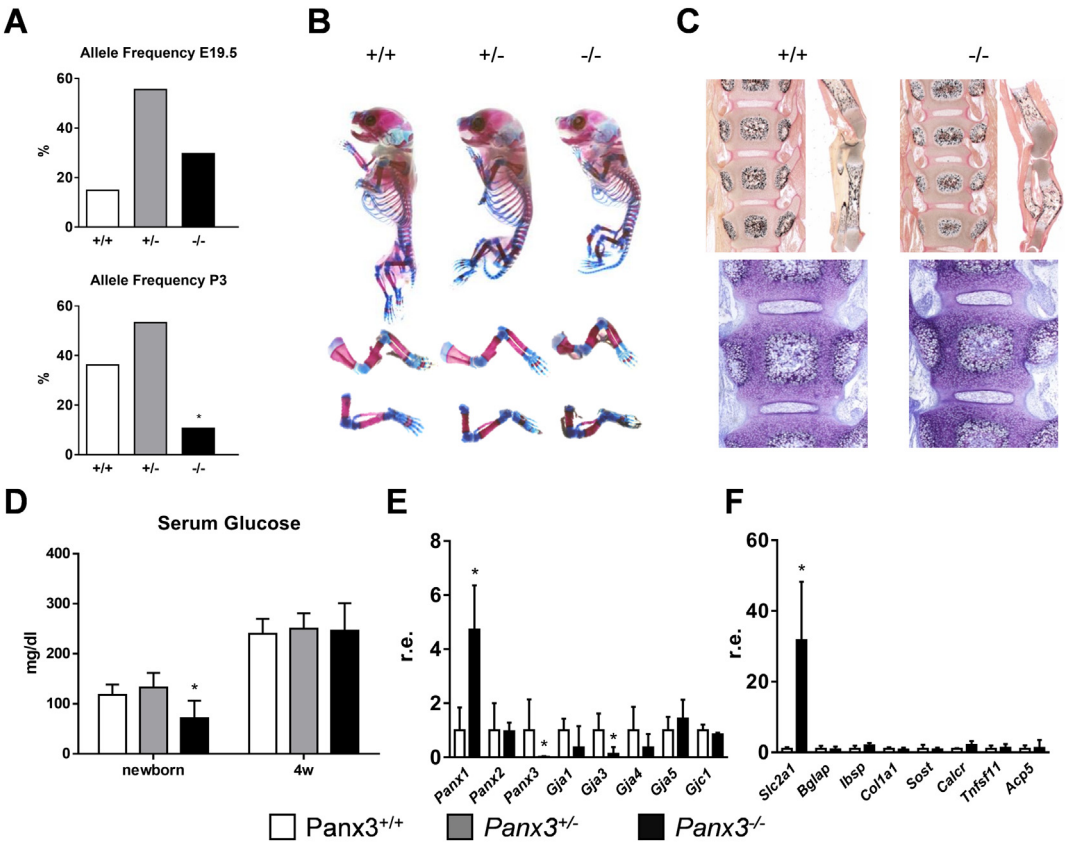

Fig. 5. Perinatal mortality of *Panx3*-deficient mice. (A) Allele frequency of offspring from heterozygous matings at E19.5 and P3. Data were analyzed by Chi^2-test. *p $<$ 0.05 vs. expected Mendelian distribution. (B) Representative images of whole skeleton alcian blue/alizarin red staining of newborn mice (P1) with the indicated *Panx3* genotypes. Note the severe deformities of the long bones of *Panx3*$^{-/-}$ mice. (C) Representative undecalcified histological sections of vertebral bodies and lower extremities from newborn *Panx3*$^{+/+}$ and *Panx3*$^{-/-}$ mice. Upper images: von Kossa/van Gieson-stain. Lower images: toluidine blue stain. (D) Serum glucose levels in newborn and four weeks old mice with the indicated genotypes. Data were analyzed by Student's *t*-test with Bonferroni correction for multiple testing. Newborn: n = 5 (*Panx3*$^{+/+}$), 13 (*Panx3*$^{+/-}$), 5 (*Panx3*$^{-/-}$); 4w: n = 7 (*Panx3*$^{+/+}$), 3 (*Panx3*$^{+/-}$), 5 (*Panx3*$^{-/-}$). *p $<$ 0.05 vs. *Panx3*$^{+/-}$. (E) qRT-PCR expression analysis of the indicated Panx- and connexin-encoding genes in calvarial bone from E19.5 embryos. Shown is the expression in *Panx3*$^{-/-}$ relative to *Panx3*$^{+/+}$ controls. (F) qRT-PCR expression analysis of additional genes in the same samples. Data were analyzed by Student's *t*-test. n = 4 (*Panx3*$^{+/+}$), 5 (*Panx3*$^{-/-}$).*p $<$ 0.05 vs. *Panx3*$^{+/+}$. (For interpretation of the references to colour in this figure legend, the reader is referred to the web version of this article.)

Panx1-deficient mice, which displayed increased *Panx3* expression in the vasculature [46], in skin [47], and in the vomeronasal organ [48]. On the other hand, there was an evident impact of *Panx3*-deficiency on endochondral ossification detectable immediately after birth, together with a high mortality rate. Importantly, the phenotype of mice lacking both, Panx1 and Panx3, has recently been reported [49]. Here it was found, although there was no side-by-side comparison towards mice lacking only Panx3, that the skeletal growth phenotype was not more pronounced in double-deficient mice. Moreover, determination of the weaned litter size indicated that the lethality rate of *Panx3*-deficient mice is not further increased by additional Panx1 deletion.

Although we were unable to identify the cause of this postnatal mortality, the observed hypoglycemia in newborn *Panx3*$^{-/-}$ mice, which was not found in *Panx3*$^{-/-}$ survivors at 4 weeks of age, might indicate an underlying problem in energy metabolism. Moreover, glucose uptake by cells of the osteoblast lineage is an essential early step in the differentiation process, and animals lacking Glut1 in *Sp7*-expressing cells display impaired skeletal development [33]. It was therefore remarkable that the Glut1-encoding gene *Slc2a1* was the only gene, besides *Panx1*, which was expressed at higher levels in *Panx3*$^{-/-}$ embryos at E19.5. Therefore, loss of Panx3 potentially interferes with osteoblast-regulated energy metabolism [34], which might trigger a cellular feedback mechanism leading the increased expression of *Slc2a1* to assure the energy demands of bone-forming osteoblasts. In any case, it is possible that a compensatory induction of Panx1 attenuates the severity of the *Panx3*$^{-/-}$ phenotype, since all *Panx3*-deficient mice that survived the first days after birth, did not develop a detectable phenotype of bone remodeling and glucose homeostasis. In our opinion, it would be extremely informative to study the respective parameters in the newly developed mouse model with combined deficiency of Panx1 and Panx3.

Supplementary data to this article can be found online at https://doi.org/10.1016/j.bone.2019.06.008.

Acknowledgements

We would like to thank the UKE research animal facility and the UKE microarray core facility for their services. Moreover we would like to express our gratitude to Lana Rosenthal, Olga Winter, Mona Neven and Elke Leicht for their technical assistance and Susan Amirbeigiarab, Tina Wallaschkowski and Tonia Bargmann for their assistance during their internship.

Authors' roles: Study design: TAY and TS. Study conduct: TAY and SP. Data interpretation: TAY, MA, TS. Drafting manuscript: TAY and TS. Revising manuscript: all authors. Approving manuscript for publication: all authors.

References

[1] P. Katsimbri, The biology of normal bone remodelling, Eur. J. Cancer Care (Engl.) 26 (6) (2017).

[2] M. Capulli, R. Paone, N. Rucci, Osteoblast and osteocyte: games without frontiers, Arch. Biochem. Biophys. 561 (2014) 3–12.
[3] S.L. Teitelbaum, Bone resorption by osteoclasts, Science 289 (5484) (2000) 1504–1508.
[4] J.E. Compston, M.R. McClung, W.D. Leslie, Osteoporosis, Lancet 393 (10169) (2019) 364–376.
[5] B.Z. Leder, ptimizing sequential and combined anabolic and antiresorptive osteoporosis therapy, JBMR Plus 2 (2) (2018) 62–68.
[6] A.B. Hodsman, D.C. Bauer, D.W. Dempster, L. Dian, D.A. Hanley, S.T. Harris, D.L. Kendler, M.R. McClung, P.D. Miller, W.P. Olszynski, E. Orwoll, C.K. Yuen, Parathyroid hormone and teriparatide for the treatment of osteoporosis: a review of the evidence and suggested guidelines for its use, Endocr. Rev. 26 (5) (2005) 688–703.
[7] K.N. Tu, J.D. Lie, C.K.V. Wan, M. Cameron, A.G. Austel, J.K. Nguyen, K. Van, D. Hyun, Osteoporosis: a review of treatment options, P T 43 (2) (2018) 92–104.
[8] S. Aggarwal, SSkeletal dysplasias with increased bone density: evolution of molecular pathogenesis in the last century, Gene 528 (1) (2013) 41–45.
[9] D.L. Lacey, W.J. Boyle, W.S. Simonet, P.J. Kostenuik, W.C. Dougall, J.K. Sullivan, J. San Martin, R. Dansey, Bench to bedside: elucidation of the OPG-RANK-RANKL pathway and the development of denosumab, Nat. Rev. Drug Discov. 11 (5) (2012) 401–419.
[10] R. Baron, M. Kneissel, WNT signaling in bone homeostasis and disease: from human mutations to treatments, Nat. Med. 19 (2) (2013) 179–192.
[11] M.R. McClung, Sclerostin antibodies in osteoporosis: latest evidence and therapeutic potential, Ther. Adv. Musculoskelet. Dis. 9 (10) (2017) 263–270.
[12] N. Vollersen, I. Hermans-Borgmeyer, K. Cornils, B. Fehse, T. Rolvien, I. Triviai, A. Jeschke, R. Oheim, M. Amling, T. Schinke, T.A. Yorgan, High bone turnover in mice carrying a pathogenic Notch2 mutation causing Hajdu-Cheney syndrome, J. Bone Miner. Res. 33 (1) (2018) 70–83.
[13] A. Jeschke, P. Catala-Lehnen, S. Sieber, T. Bickert, M. Schweizer, T. Koehne, K. Wintges, R.P. Marshall, A. Mautner, L. Duchstein, B. Otto, A.K. Horst, M. Amling, H.J. Kreienkamp, T. Schinke, harpin controls osteogenic differentiation of mesenchymal bone marrow cells, J. Immunol. 195 (8) (2015) 3675–3684.
[14] M.K. Chang, L.J. Raggatt, K.A. Alexander, J.S. Kuliwaba, N.L. Fazzalari, K. Schroder, E.R. Maylin, V.M. Ripoll, D.A. Hume, A.R. Pettit, Osteal tissue macrophages are intercalated throughout human and mouse bone lining tissues and regulate osteoblast function in vitro and in vivo, J. Immunol. 181 (2) (2008) 1232–1244.
[15] R. Edgar, M. Domrachev, A.E. Lash, Gene Expression Omnibus: NCBI gene expression and hybridization array data repository, Nucleic Acids Res. 30 (1) (2002) 207–210.
[16] A. Rauch, S. Seitz, U. Baschant, A.F. Schilling, A. Illing, B. Stride, M. Kirilov, V. Mandic, A. Takacz, R. Schmidt-Ullrich, S. Ostermay, T. Schinke, R. Spanbroek, M.M. Zaiss, P.E. Angel, U.H. Lerner, J.P. David, H.M. Reichardt, M. Amling, G. Schutz, J.P. Tuckermann, Glucocorticoids suppress bone formation by attenuating osteoblast differentiation via the monomeric glucocorticoid receptor, Cell Metab. 11 (6) (2010) 517–531.
[17] J. Luther, T.A. Yorgan, T. Rolvien, L. Ulsamer, T. Koehne, N. Liao, D. Keller, N. Vollersen, S. Teufel, M. Neven, S. Peters, M. Schweizer, A. Trumpp, S. Rosigkeit, E. Bockamp, S. Mundlos, U. Kornak, R. Oheim, M. Amling, T. Schinke, J.P. David, Wnt1 is an Lrp5-independent bone-anabolic Wnt ligand, Sci. Transl. Med. 10 (466) (2018).
[18] A. Bartelt, F. Behler-Janbeck, F.T. Beil, T. Koehne, B. Muller, T. Schmidt, M. Heine, L. Ochs, T. Yilmaz, M. Dietrich, J.P. Tuckermann, M. Amling, J. Herz, T. Schinke, J. Heeren, A. Niemeier, Lrp1 in osteoblasts controls osteoclast activity and protects against osteoporosis by limiting PDGF-RANKL signaling, Bone Res. 6 (2018) 4.
[19] T. Yorgan, N. Vollersen, C. Riedel, A. Jeschke, S. Peters, B. Busse, M. Amling, T. Schinke, Osteoblast-specific Notch2 inactivation causes increased trabecular bone mass at specific sites of the appendicular skeleton, Bone 87 (2016) 136–146.
[20] S. Seitz, J. Keller, A.F. Schilling, A. Jeschke, R.P. Marshall, B.D. Stride, T. Wintermantel, F.T. Beil, M. Amling, G. Schutz, J. Tuckermann, T. Schinke, Pharmacological estrogen administration causes a FSH-independent osteo-anabolic effect requiring ER alpha in osteoblasts, PLoS One 7 (11) (2012) e50301.
[21] J. Keller, P. Catala-Lehnen, A.K. Huebner, A. Jeschke, T. Heckt, A. Lueth, M. Krause, T. Koehne, J. Albers, J. Schulze, S. Schilling, M. Haberland, H. Denninger, M. Neven, I. Hermans-Borgmeyer, T. Streichert, S. Breer, F. Barvencik, B. Levkau, B. Rathkolb, E. Wolf, J. Calzada-Wack, F. Neff, V. Gailus-Durner, H. Fuchs, M.H. de Angelis, S. Klutmann, E. Tsourdi, L.C. Hofbauer, B. Kleuser, J. Chun, T. Schinke, M. Amling, Calcitonin controls bone formation by inhibiting the release of sphingosine 1-phosphate from osteoclasts, Nat. Commun. 5 (2014) 5215.
[22] T.A. Yorgan, S. Peters, A. Jeschke, P. Benisch, F. Jakob, M. Amling, T. Schinke, The anti-osteoanabolic function of sclerostin is blunted in mice carrying a high bone mass mutation of Lrp5, J. Bone Miner. Res. 30 (7) (2015) 1175–1183.
[23] M.L. Bouxsein, S.K. Boyd, B.A. Christiansen, R.E. Guldberg, K.J. Jepsen, R. Muller, Guidelines for assessment of bone microstructure in rodents using micro-computed tomography, J. Bone Miner. Res. 25 (7) (2010) 1468–1486.
[24] J. Albers, J. Keller, A. Baranowsky, F.T. Beil, P. Catala-Lehnen, J. Schulze, M. Amling, T. Schinke, Canonical Wnt signaling inhibits osteoclastogenesis independent of osteoprotegerin, J. Cell Biol. 200 (4) (2013) 537–549.
[25] D.W. Dempster, J.E. Compston, M.K. Drezner, F.H. Glorieux, J.A. Kanis, H. Malluche, P.J. Meunier, S.M. Ott, R.R. Recker, A.M. Parfitt, Standardized nomenclature, symbols, and units for bone histomorphometry: a 2012 update of the report of the ASBMR Histomorphometry Nomenclature Committee, J. Bone Miner. Res. 28 (1) (2013) 2–17.
[26] L. Beck, Y. Soumounou, J. Martel, G. Krishnamurthy, C. Gauthier, C.G. Goodyer, H.S. Tenenhouse, Pex/PEX tissue distribution and evidence for a deletion in the 3′ region of the Pex gene in X-linked hypophosphatemic mice, J. Clin. Invest. 99 (6) (1997) 1200–1209.
[27] N. Hanagata, X. Li, H. Morita, T. Takemura, J. Li, T. Minowa, Characterization of the osteoblast-specific transmembrane protein IFITM5 and analysis of IFITM5-deficient mice, J. Bone Miner. Metab. 29 (3) (2011) 279–290.
[28] N.A. Sims, C.P. White, K.L. Sunn, G.P. Thomas, M.L. Drummond, N.A. Morrison, J.A. Eisman, E.M. Gardiner, Human and murine osteocalcin gene expression: conserved tissue restricted expression and divergent responses to 1,25-dihydroxyvitamin D3 in vivo, Mol. Endocrinol. 11 (11) (1997) 1695–1708.
[29] S.K. Oh, J.O. Shin, J.I. Baek, J. Lee, J.W. Bae, H. Ankamerddy, M.J. Kim, T.L. Huh, Z.Y. Ryoo, U.K. Kim, J. Bok, K.Y. Lee, Pannexin 3 is required for normal progression of skeletal development in vertebrates, FASEB J. 29 (11) (2015) 4473–4484.
[30] M. Ishikawa, G.L. Williams, T. Ikeuchi, K. Sakai, S. Fukumoto, Y. Yamada, Pannexin 3 and connexin 43 modulate skeletal development through their distinct functions and expression patterns, J. Cell Sci. 129 (5) (2016) 1018–1030.
[31] N.K. Lee, H. Sowa, E. Hinoi, M. Ferron, J.D. Ahn, C. Confavreux, R. Dacquin, P.J. Mee, M.D. McKee, D.Y. Jung, Z. Zhang, J.K. Kim, F. Mauvais-Jarvis, P. Ducy, G. Karsenty, Endocrine regulation of energy metabolism by the skeleton, Cell 130 (3) (2007) 456–469.
[32] J.P. Stains, R. Civitelli, Connexins in the skeleton, Semin. Cell Dev. Biol. 50 (2016) 31–39.
[33] J. Wei, J. Shimazu, M.P. Makinistoglu, A. Maurizi, D. Kajimura, H. Zong, T. Takarada, T. Lezaki, J.E. Pessin, E. Hinoi, G. Karsenty, Glucose uptake and Runx2 synergize to orchestrate osteoblast differentiation and bone formation, Cell 161 (7) (2015) 1576–1591.
[34] G. Karsenty, M. Ferron, The contribution of bone to whole-organism physiology, Nature 481 (7381) (2012) 314–320.
[35] K. Nakashima, X. Zhou, G. Kunkel, Z. Zhang, J.M. Deng, R.R. Behringer, B. de Crombrugghe, The novel zinc finger-containing transcription factor osterix is required for osteoblast differentiation and bone formation, Cell 108 (1) (2002) 17–29.
[36] X. Li, M.S. Ominsky, Q.T. Niu, N. Sun, B. Daugherty, D. D'Agostin, C. Kurahara, Y. Gao, J. Cao, J. Gong, F. Asuncion, M. Barrero, K. Warmington, D. Dwyer, M. Stolina, S. Morony, I. Sarosi, P.J. Kostenuik, D.L. Lacey, W.S. Simonet, H.Z. Ke, C. Paszty, Targeted deletion of the sclerostin gene in mice results in increased bone formation and bone strength, J. Bone Miner. Res. 23 (6) (2008) 860–869.
[37] M.R. McClung, A. Grauer, S. Boonen, M.A. Bolognese, J.P. Brown, A. Diez-Perez, B.L. Langdahl, J.Y. Reginster, J.R. Zanchetta, S.M. Wasserman, L. Katz, J. Maddox, Y.C. Yang, C. Libanati, H.G. Bone, Romosozumab in postmenopausal women with low bone mineral density, N. Engl. J. Med. 370 (5) (2014) 412–420.
[38] E.M. Lewiecki, R.V. Dinavahi, M. Lazaretti-Castro, P.R. Ebeling, J.D. Adachi, A. Miyauchi, E. Gielen, C.E. Milmont, C. Libanati, A. Grauer, One year of romosozumab followed by two years of denosumab maintains fracture risk reductions: results of the FRAME extension study, J. Bone Miner. Res. 34 (3) (2018) 419–428.
[39] B. Pietrzyk, M. Smertka, J. Chudek, Sclerostin: intracellular mechanisms of action and its role in the pathogenesis of skeletal and vascular disorders, Adv. Clin. Exp. Med. 26 (8) (2017) 1283–1291.
[40] M.M. Weivoda, S.J. Youssef, M.J. Oursler, Sclerostin expression and functions beyond the osteocyte, Bone 96 (2017) 45–50.
[41] T. Iwamoto, T. Nakamura, A. Doyle, M. Ishikawa, S. de Vega, S. Fukumoto, Y. Yamada, Pannexin 3 regulates intracellular ATP/cAMP levels and promotes chondrocyte differentiation, J. Biol. Chem. 285 (24) (2010) 18948–18958.
[42] M. Ishikawa, T. Iwamoto, T. Nakamura, A. Doyle, S. Fukumoto, Y. Yamada, Pannexin 3 functions as an ER Ca(2+) channel, hemichannel, and gap junction to promote osteoblast differentiation, J. Cell Biol. 193 (7) (2011) 1257–1274.
[43] P.M. Moon, S. Penuela, K. Barr, S. Khan, C.L. Pin, I. Welch, M. Attur, S.B. Abramson, D.W. Laird, F. Beier, Deletion of Panx3 prevents the development of surgically induced osteoarthritis, J. Mol. Med. (Berl.) 93 (8) (2015) 845–856.
[44] D. Caskenette, S. Penuela, V. Lee, K. Barr, F. Beier, D.W. Laird, K.E. Willmore, Global deletion of Panx3 produces multiple phenotypic effects in mouse humeri and femora, J. Anat. 228 (5) (2016) 746–756.
[45] S.R. Bond, A. Lau, S. Penuela, A.V. Sampaio, T.M. Underhill, D.W. Laird, C.C. Naus, Pannexin 3 is a novel target for Runx2, expressed by osteoblasts and mature growth plate chondrocytes, J. Bone Miner. Res. 26 (12) (2011) 2911–2922.
[46] A.W. Lohman, M. Billaud, A.C. Straub, S.R. Johnstone, A.K. Best, M. Lee, K. Barr, S. Penuela, D.W. Laird, B.E. Isakson, Expression of pannexin isoforms in the systemic murine arterial network, J. Vasc. Res. 49 (5) (2012) 405–416.
[47] S. Penuela, J.J. Kelly, J.M. Churko, K.J. Barr, A.C. Berger, D.W. Laird, Panx1 regulates cellular properties of keratinocytes and dermal fibroblasts in skin development and wound healing, J. Invest. Dermatol. 134 (7) (2014) 2026–2035.
[48] P. Whyte-Fagundes, S. Kurtenbach, C. Zoidl, V.I. Shestopalov, P.L. Carlen, G. Zoidl, A potential compensatory role of Panx3 in the VNO of a Panx1 knock out mouse model, Front. Mol. Neurosci. 11 (2018) 135.
[49] J.M. Abitbol, B.L. O'Donnell, C.B. Wakefield, E. Jewlal, J.J. Kelly, K. Barr, K.E. Willmore, B.L. Allman, S. Penuela, Double deletion of Panx1 and Panx3 affects skin and bone but not hearing, J. Mol. Med. (Berl.) 97 (5) (2019) 723–736.